

# $\alpha$ -Bi<sub>2</sub>Sn<sub>2</sub>O<sub>7</sub>: A Potential Room Temperature *n*-type Oxide Thermoelectric — Supplementary Information

Warda Rahim,<sup>\*,†,‡</sup> Jonathan M. Skelton,<sup>¶</sup> and David O. Scanlon<sup>\*,†,‡,§</sup>

<sup>†</sup>*Department of Chemistry, University College London, 20 Gordon Street, London WC1H  
0AJ, UK*

<sup>‡</sup>*Thomas Young Centre, University College London, Gower Street, London WC1E 6BT,  
UK*

<sup>¶</sup>*School of Chemistry, University of Manchester, Oxford Road, Manchester M13 9PL, UK*

<sup>§</sup>*Diamond Light Source Ltd., Diamond House, Harwell Science and Innovation Campus,  
Didcot, Oxfordshire OX11 0DE, UK*

E-mail: warda.rahim.18@ucl.ac.uk; d.scanlon@ucl.ac.uk

# Convergence of the Total Energy with the Plane-wave Cutoff and $k$ -point Sampling

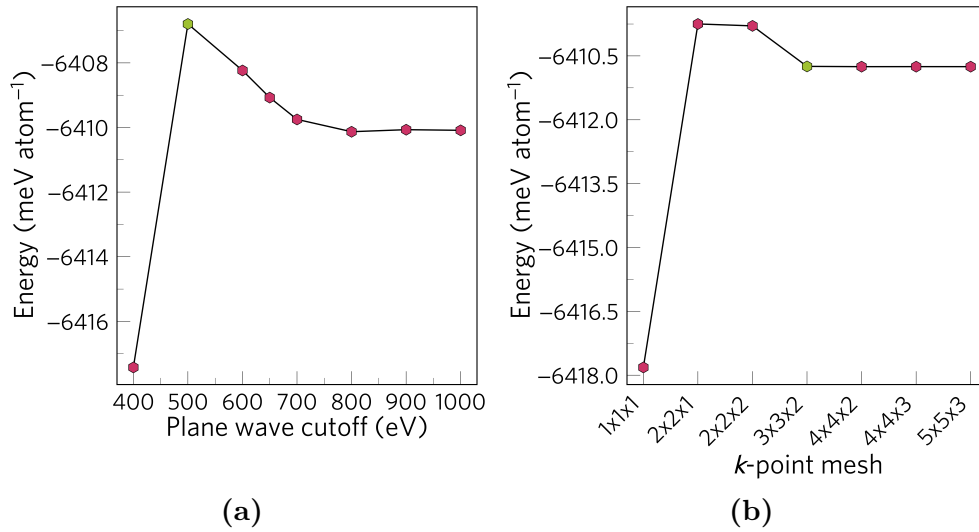


**Figure S1:** Calculated total energy of  $\alpha$ - $\text{Bi}_2\text{Sn}_2\text{O}_7$  as a function of (a) plane wave kinetic-energy cutoff and (b)  $k$ -point sampling mesh. The values converged to 3 meV per atom for the cutoff, and 1 meV per atom for the  $k$ -point mesh are highlighted in green.

# Comparison of the HSE06 Electronic Band Structure with and without Spin-Orbit Coupling Effects

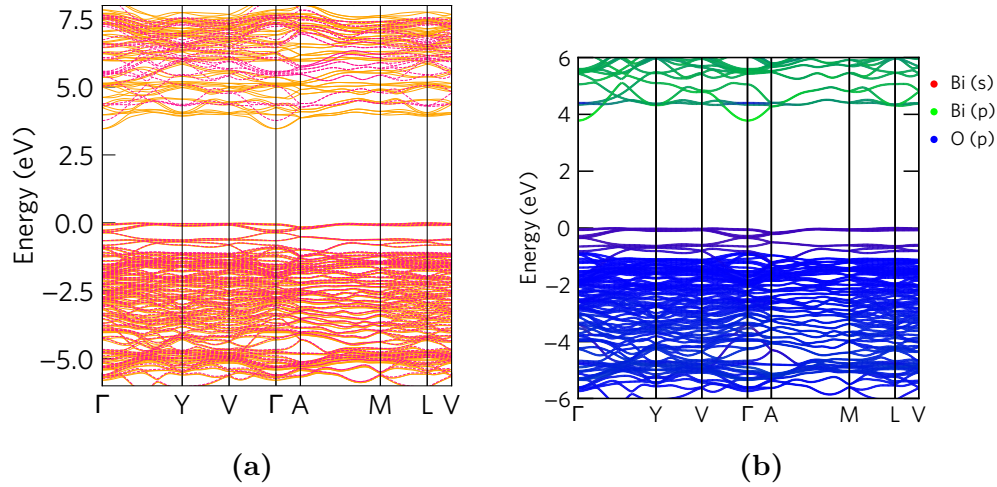


**Figure S2:** (a) Calculated HSE06 electronic band structure of  $\alpha$ - $\text{Bi}_2\text{Sn}_2\text{O}_7$  with and without spin-orbit coupling (SOC) effects, shown in solid orange and dashed pink lines, respectively, showing major changes at the bottom of the conduction band (CB) due to the presence of Bi 6p states and negligible changes at the top of the valence band (VB), composed of Bi 6s (no SOC effect) and O 2p states (no relativistic effect). (b) Orbital-projected HSE06 + SOC band structure showing that the conduction band minimum (CBM) is composed mainly of Bi 6p states (green lines), and the valence band maximum (VBM) is a mixture of Bi 6s and O 2p states (purple lines). The VBM in both (a) and (b) is set to  $E = 0$  eV.

# Convergence of the Phonon Frequencies with Supercell Expansion

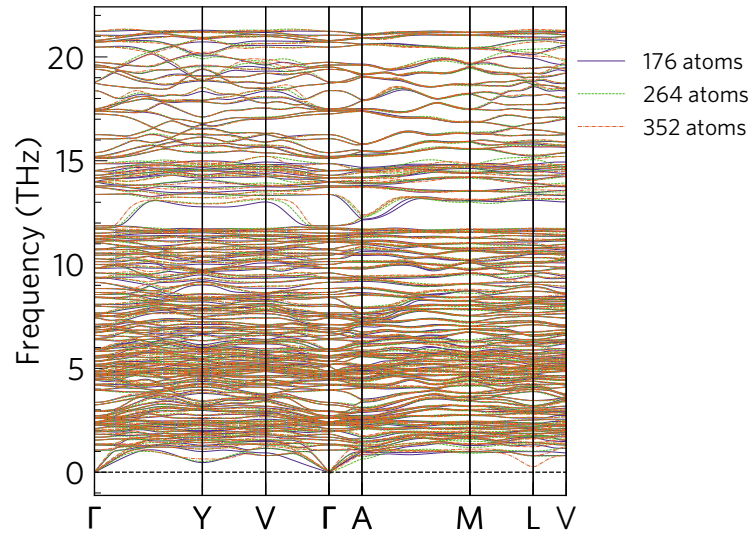
The harmonic phonon dispersion of  $\alpha$ -Bi<sub>2</sub>Sn<sub>2</sub>O<sub>7</sub> was explicitly converged with respect to the supercell expansion. Since the structure has a 44-atom primitive cell, supercell expansions larger than  $2 \times 2 \times 2$  (352 atoms) would be computationally very expensive. We therefore used non-diagonal supercell matrices to generate cubic supercells from the primitive cell according to the relation given in Eq. (1):

$$(a_s b_s c_s) = (a_u b_u c_u) M_s \quad (1)$$

where,  $M_s$  is the supercell matrix, the lattice parameters of unit cell are given by a column vector with components  $a_u, b_u, c_u$ , and those of supercell are given by a vector with components  $a_s, b_s, c_s$ .

The supercell matrices used are listed in Eq. (2) and result in supercells with 176, 264 and 352 atoms. Figure S3 shows how the harmonic phonon frequencies vary with the supercell size. There is little difference between the phonon dispersion curves obtained using the 264- and 352-atom supercells, so we therefore decided to use the 264 atom supercell for the calculation of the harmonic force constants.

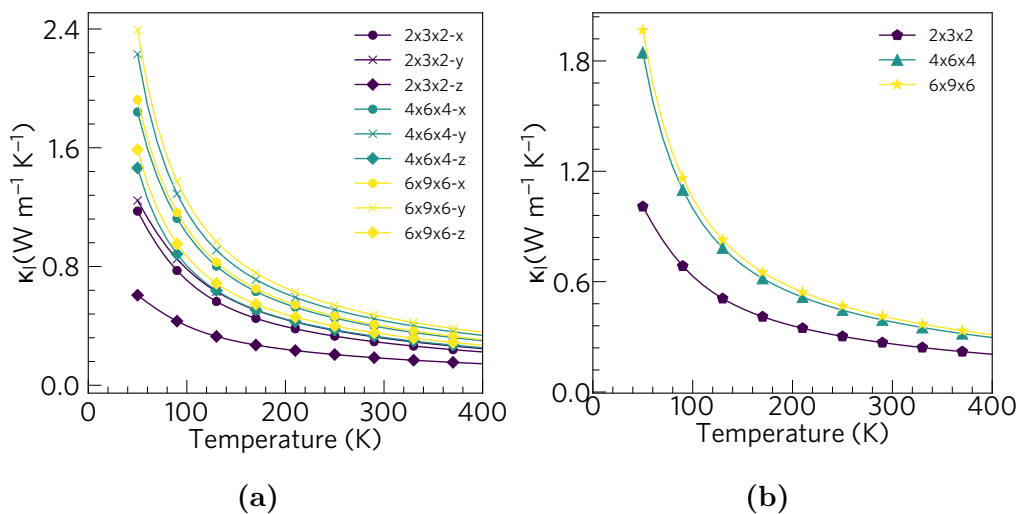
$$\begin{bmatrix} 2 & 2 & -1 \\ 2 & 0 & 0 \\ 0 & 0 & -1 \end{bmatrix}, \begin{bmatrix} 2 & 1 & 0 \\ 0 & 1 & 2 \\ 1 & -1 & 0 \end{bmatrix}, \begin{bmatrix} 3 & 0 & 0 \\ 1 & 2 & 1 \\ 0 & -1 & 1 \end{bmatrix} \quad (2)$$



**Figure S3:** Harmonic phonon dispersion curves of  $\alpha$ - $\text{Bi}_2\text{Sn}_2\text{O}_7$  obtained using a range of supercell expansions to calculate the second-order force constants.

## Convergence of $\kappa_l$ with $q$ -point Sampling Mesh

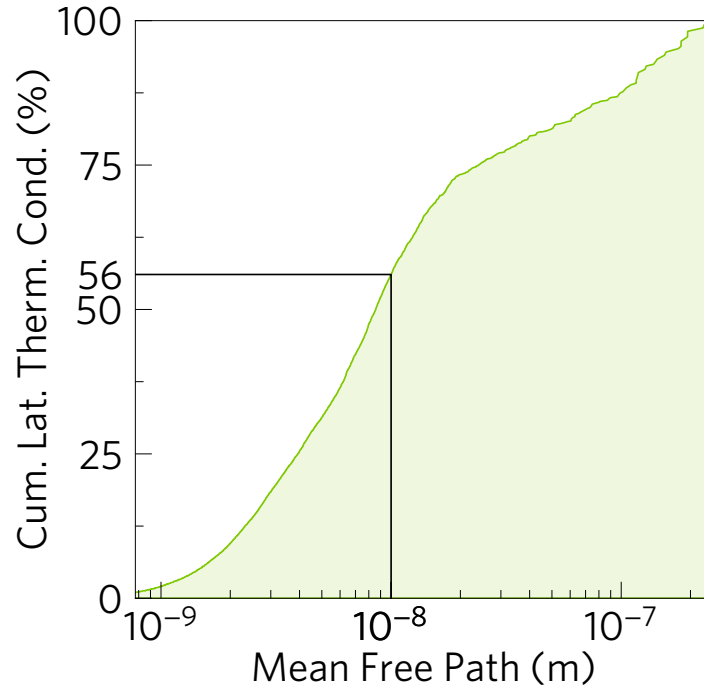
Figure S4 shows the convergence of the  $xx$ ,  $yy$  and  $zz$  components of the  $\kappa_l$  tensor and the isotropically averaged  $\kappa_l$  values with respect to the  $q$ -point mesh used to sample the phonon Brillouin zone. The percentage difference between the  $\kappa_l$  obtained using the  $4 \times 6 \times 4$  and  $6 \times 9 \times 6$  meshes is relatively small ( $< 3\%$  for  $\kappa_{xx}$ ,  $< 7\%$  for  $\kappa_{yy}$  and  $\kappa_{zz}$ , and  $5\%$  for  $\kappa_{iso}$  at 300 K).



**Figure S4:** (a) Convergence of the principal  $xx$ ,  $yy$  and  $zz$  components of the  $\kappa_l$  tensor as a function of temperature with the  $q$ -point sampling mesh. (b) Convergence of the isotropically-averaged  $\kappa_l$  with  $q$ -point sampling.

# Cumulative $\kappa_l$ as a Function of the Phonon Mean Free Path

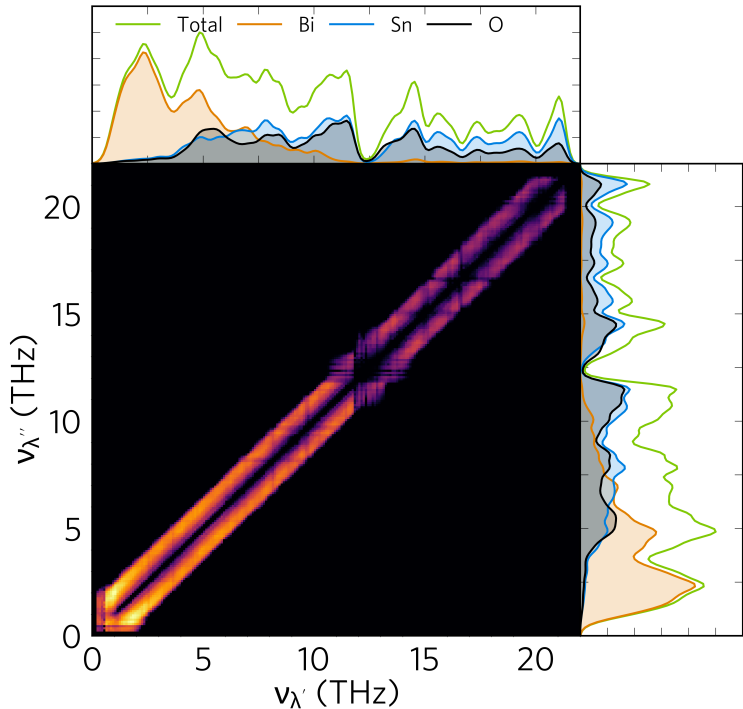
The cumulative  $\kappa_l$  of  $\alpha$ -Bi<sub>2</sub>Sn<sub>2</sub>O<sub>7</sub> as a function of the phonon mean free path is shown in Figure S5. The solid lines indicate that 56% of the heat is carried by phonons with a mean free path of < 10 nm. This indicates that nanostructuring to 10 nm or lower, if possible, could help to further suppress the heat transport.



**Figure S5:** Cumulative 300 K lattice thermal conductivity as a function of phonon mean free path for  $\alpha$ -Bi<sub>2</sub>Sn<sub>2</sub>O<sub>7</sub>. The black line marked on the plot shows that 56% of heat is carried by phonons with mean free paths < 10 nm.

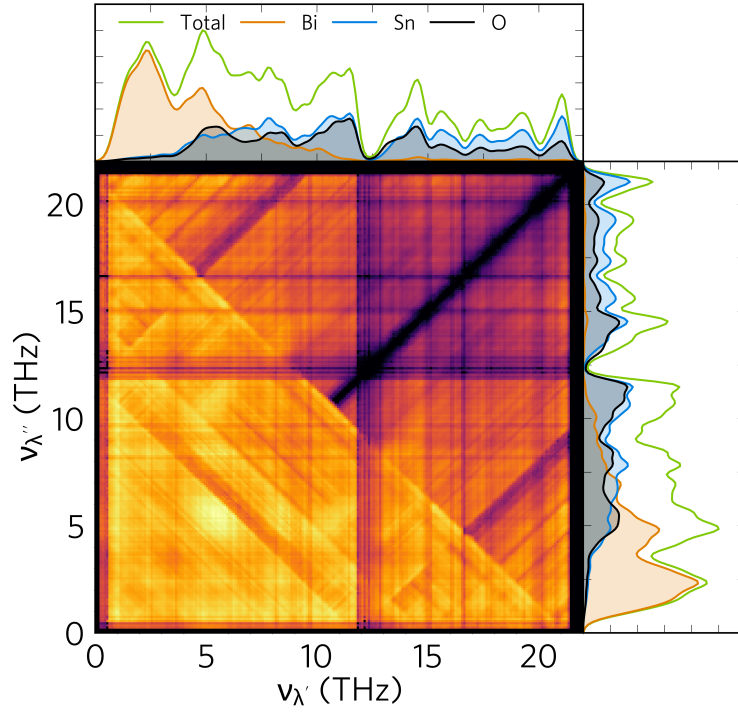
# Modal Contributions to the Phonon Linewidths

Figure S6 shows the pairwise contributions of modes to the line broadening of the acoustic modes. As discussed in the text, collisions with other acoustic modes and low-lying optic modes are the dominant scattering mechanism for these modes, followed by interactions with mid-frequency optic modes. The higher-frequency optic modes involving the motion of Sn and O atoms also contribute but far less than the low-frequency modes.



**Figure S6:** 2D histogram showing the pairwise contributions of modes with frequencies  $\nu'_\lambda$  and  $\nu''_\lambda$  to the linewidths of the acoustic modes with  $\nu < 1.3$  THz, in  $\alpha$ - $\text{Bi}_2\text{Sn}_2\text{O}_7$ . This plot covers the full range of the phonon spectrum and may be compared to Figure 10 in the text.

The 2D histogram in Figure S7 shows the pairwise contributions to the line broadening over the entire  $\alpha$ - $\text{Bi}_2\text{Sn}_2\text{O}_7$  spectrum. This again shows that scattering with acoustic and low-frequency optic modes up to 5 THz makes the largest contribution to the line broadening. These low-frequency modes are dominated by vibrations of the Bi atoms, highlighting the role of the Bi cations in suppressing the thermal transport in the structure.



**Figure S7:** 2D histogram showing the pairwise contributions of modes with frequencies  $\nu'_\lambda$  and  $\nu''_\lambda$  to the linewidths of modes across the full range of the  $\alpha$ - $\text{Bi}_2\text{Sn}_2\text{O}_7$  phonon spectrum.